

## Accepted Manuscript

Textural development in sulfide-matrix ore breccias in the Aguablanca Ni-Cu deposit, Spain, revealed by X-ray fluorescence microscopy

Stephen J. Barnes, Rubén Piña, Margaux Le Vaillant

PII: S0169-1368(17)30912-5  
DOI: <https://doi.org/10.1016/j.oregeorev.2018.03.004>  
Reference: OREGEO 2520

To appear in: *Ore Geology Reviews*

Received Date: 25 November 2017  
Revised Date: 28 February 2018  
Accepted Date: 5 March 2018

Please cite this article as: S.J. Barnes, R. Piña, M. Le Vaillant, Textural development in sulfide-matrix ore breccias in the Aguablanca Ni-Cu deposit, Spain, revealed by X-ray fluorescence microscopy, *Ore Geology Reviews* (2018), doi: <https://doi.org/10.1016/j.oregeorev.2018.03.004>

This is a PDF file of an unedited manuscript that has been accepted for publication. As a service to our customers we are providing this early version of the manuscript. The manuscript will undergo copyediting, typesetting, and review of the resulting proof before it is published in its final form. Please note that during the production process errors may be discovered which could affect the content, and all legal disclaimers that apply to the journal pertain.



## Textural development in sulfide-matrix ore breccias in the Aguablanca Ni-Cu deposit, Spain, revealed by X-ray fluorescence microscopy

Stephen J. Barnes<sup>1</sup>, Rubén Piña<sup>2</sup>, Margaux Le Vaillant<sup>1</sup>

<sup>1</sup>CSIRO Mineral Resources, Perth, Australia. [steve.barnes@csiro.au](mailto:steve.barnes@csiro.au); [margaux.levaillant@csiro.au](mailto:margaux.levaillant@csiro.au)

<sup>2</sup>Department of Mineralogy and Petrology, Faculty of Geological Science, University Complutense of Madrid, Spain, [rpinagar@ucm.es](mailto:rpinagar@ucm.es)

### Abstract

The intrusion-hosted Ni-Cu sulfide deposit at Aguablanca in south-western Spain contains a high proportion of ores in the form of sulfide-matrix ore breccias. These are polymict, with autolith and xenolith inclusions in sulfide-rich and/or sulfide-poor matrices. Inclusion lithologies include calc-silicate skarn rocks from the adjacent marbles, ultramafic and mafic cumulates, and remelted and recrystallized mafic rocks containing spinifex-like textures.

Breccia textures have been investigated at mm to cm scale using desk-top and synchrotron-based microbeam XRF mapping which reveals a number of distinctive common features: disaggregation of inclusions into adjacent sulfide along original silicate grain boundaries; complex reverse and oscillatory zoning in Cr content of clinopyroxene grains within sulfide and inside inclusions; narrow reaction rims between country rock clasts and enclosing silicates; and preferential disposition of pyroxene crystals within pyrrhotite-pentlandite aggregates (original MSS) relative to inclusion-poor chalcopyrite.

The observed range of textures is explained by a model of percolation of molten sulfide through a pre-existing silicate-matrix intrusion breccia, preferentially displacing a cotectic or eutectic plagioclase-pyroxene melt. The process is analogous to that believed to have formed interspinifex ore in komatiite-hosted deposits, and also to that responsible for superficially similar sulfide matrix ore breccias at Voisey's Bay. The preserved range of textures is interpreted as being due to late stage gravity-driven percolation of sulfide liquid from above into a pre-existing partially molten intrusion breccia. This intrusion breccia itself may have been emplaced into the neck of the Aguablanca stock, in the waning stages of magma flow.

*Keywords: Nickel, magmatic sulfide, intrusion, emplacement, infiltration, percolation*

## 1. Introduction

Magmatic Ni-Cu-PGE sulfide ores hosted in small mafic-ultramafic conduit-style intrusions commonly contain a high proportion of sulfide-matrix breccias; assemblages of silicate rock inclusions within a matrix of original magmatic sulfide liquid. Such ore types have been widely recognised and reported, but with a few exceptions (Ripley and Alawi, 1988; Arcuri et al., 1998; Li and Naldrett, 2000; Mariga et al., 2006; Piña et al., 2006; Barnes et al., 2017a) have received little detailed study.

Sulfide-matrix breccia ores are common features of deposits hosted within intrusions formed from mafic magmas, but are less prevalent in komatiite hosted deposits. They account for a large proportion of sulfide-rich ores in a number of deposits, including many of the sub-layer and offset dyke deposits at Sudbury (Lightfoot et al., 1997; Lightfoot and Farrow, 2002; Lightfoot, 2016), deep portions of the feeder dyke system and margins of the Ovoid and Eastern Deeps orebodies at Voisey's Bay (Lightfoot et al., 2012; Barnes et al., 2017a), several of the small mafic-ultramafic intrusion hosted deposits in central Finland (Makkonen, 2015), Savannah (formerly Sally Malay) (Hicks et al., 2017), Radio Hill (De Angelis et al., 1987) and Nebo-Babel (Seat et al., 2007) in Western Australia, and particularly in the subject of this contribution, the Aguablanca deposit in south-western Spain (Casquet et al., 2001; Tornos et al., 2001; Ortega et al., 2004; Piña et al., 2006; Tornos et al., 2006).

Genetic interpretations of sulfide matrix breccias have fallen into four main categories: tectonic "durchbewegung" origins (Marshall and Gilligan, 1989); upward emplacement of sulfide-rich slurries due to late stage compression in intrusive complexes (Evans-Lamswood et al., 2000; Ortega et al., 2004); downward emplacement as sulfide-rich gravity flows during backflow in sill-dyke complexes (Barnes et al., 2016b) or into footwall offset dykes (Lightfoot and Farrow, 2002), and gravity-driven downward percolation of sulfide liquid through the matrix of original silicate-matrix intrusion breccias (Barnes et al., 2017a).

Durchbewegung breccias can generally be distinguished on the basis of penetrative deformation fabrics and piercement structures (cross-cutting of pre-existing country rock layering by foliated sulfide) (Marshall and Gilligan, 1989) are mainly characteristic of deposits where there has been significant post emplacement tectonism, such as at Thompson, Manitoba (Lightfoot et al., 2017) in or components of such breccias are common even in weakly deformed deposits owing to the high ductility of sulfides. However, the presence of delicately-preserved igneous textures in the Voisey's Bay breccias are compelling evidence for a primary magmatic origin.

This study makes extensive use of the technique of microbeam XRF mapping (Barnes et al., 2016), to reveal petrographic features, textures and chemical zoning patterns in Aguablanca sulfide-matrix breccia ores at a scale of mm-cm. This scale is intermediate between the microscopic thin-section scale and the drill core/outcrop to mine scale at which geological relationships are most commonly viewed, and provides an effective method of visualizing the distribution of clast types, sulfides and accessory minerals.

## 2. Geological setting

The Aguablanca Ni-Cu sulfide ores occur within the Aguablanca mafic stock ( $341 \pm 1.5$  Ma, U-Pb ID-TIMS on magmatic zircons (Romeo et al., 2006)), a small ( $\sim 3$  km<sup>2</sup> in area) cylindrical to funnel shaped intrusion situated adjacent to the Cherneca ductile shear zone (Fig. 1). The Aguablanca stock forms part of the Santa Olalla Igneous Complex. This is a calc-alkaline plutonic group formed by two main plutons (Aguablanca and Santa Olalla) and other smaller intrusive bodies (Sultana, Teuler and Garrote intrusions) (Romeo et al., 2006) cropping out in the southern limb of the WNW-ESE-trending Olivenza-Monesterio antiform within the Ossa-Morena Zone of the Iberian Massif.

*Figure 1.*

At the NW margin, the Santa Olalla Igneous Complex intruded pyrite-rich black slates and metagreywackes with minor intercalations of metavolcanic rocks and black quartzites from the Tentudia succession  $564 \pm 9$  Ma old (Schäfer et al., 1993), forming the upper part of the Late Neoproterozoic Serie Negra Formation. This Formation is considered to be the source for the Aguablanca mineralization (Casquet et al., 2001; Tornos et al., 2001; Piña et al., 2006). At the E and W, the Santa Olalla Igneous Complex intruded a volcano-sedimentary sequence formed by tuffs, slates, porphyritic rhyolites and carbonate rocks at the top corresponding to the Cambrian Bodonal Cala Complex ( $530 \pm 3$  Ma, U-Pb ID-TIMS on zircons, Romeo et al. 2006) that unconformably overlies the Serie Negra Formation. Along the northern contact with the Bodonal Cala carbonate rocks, there is a well-developed exoskarn ( $\sim 2$  km wide) composed of garnetite, marble and calc-silicate rocks (Velasco, 1976; Casquet, 1980), which was affected by penetrative ductile deformation related to the sinistral transpressional kinematics of the Cherneca shear zone (Romeo et al., 2007). Casquet (1980) estimated temperatures up to  $750^\circ\text{C}$  (i.e., hypersthene hornfels facies) within the aureole near to the contact with the Aguablanca stock and inferred a depth of emplacement of 1.7 to 3.5 km from metamorphic mineral equilibria.

The Aguablanca stock is composed of orthocumulate-textured hornblende-bearing gabbro and minor gabbro and norite, grading to the south into diorite and quartz diorite. It shows vertical magmatic foliations parallel to the pluton boundaries near to the N, NE and NW contact with the Bodonal-Cala rocks and predominantly subhorizontal magmatic foliations in the central part (Romeo et al., 2008). At the south, magmatic foliations are related to the magmatic structure of the surrounding Santa Olalla intrusion with N150° strike and steep dips towards the NE. 3D gravity modeling (Romeo et al., 2008) indicates that the Aguablanca stock has an inverted-drop geometry (Fig. 1B) and that the root for the intrusion, located in the northern margin of the stock adjacent to the Cherneca Fault, has a vertical wedge shape. This led these authors to conclude that the Cherneca Fault was probably the feeder structure for the Aguablanca intrusion. Crosscutting relationships between the Aguablanca stock and the Cherneca Fault (e.g., intrusive rocks cutting the mylonitic foliation in the NE contact; the exoskarn produced by Aguablanca deformed by the Cherneca deformation) suggest that the emplacement of Aguablanca took place after the onset of deformation associated with the Cherneca Fault. The long axis of the root of the Aguablanca intrusion (N65°E) is not parallel to the Cherneca Fault (N115°E) but also seems to be coincident with the orientations expected for tension cracks developed in a sinistral ductile strike-slip shear zone with the strike corresponding to the Cherneca Fault. This led Romeo et al. (2008) to propose that the Aguablanca stock, and the Ni-Cu mineralized breccia pipes, may be emplaced along successive opening hundred-metre-scale tensional fractures formed within the strain field of the Cherneca Fault. Once the magma reached its current erosion level ascending along tensional cracks, it expanded towards the SW exploiting the subhorizontal country rock foliation.

The economic Aguablanca Ni-Cu sulfide mineralization is composed of a subvertical mineralized breccia in the northern part of the Aguablanca stock, near to the sedimentary host rocks. The breccia forms a subvertical elongate funnel with a size of about 250 to 300 m wide (N-S), about 600 m long (E-W) and a dip of 70° to 80° N, open at depth. Within the breccia, the sulfide mineralization is concentrated in northward dipping and E-W-trending subvertical orebodies characterized by a variably mineralized matrix hosting unmineralized mafic-ultramafic igneous and host country rock fragments (Fig. 2). Orebodies are locally truncated by post-mineralization Variscan NE-oriented strike-slip faults. According to the sulfide abundance, two main types of ore mineralization are distinguished: semi-massive and disseminated ores. The semi-massive ore consists of up to 85 modal % sulfides, but

commonly between 20 and 70 modal %. These sulfides poikilitically enclose euhedral to subhedral crystals of olivine, pyroxene and/or plagioclase. The disseminated ore is volumetrically more abundant than the semi-massive ore and consists of sulfides (< 20 modal %) in a gabbronorite rock, for the most part conforming to the category of interstitial disseminated ores (Barnes et al., 2017b) with a less abundant component of globular ore. The ore-types are concentrically distributed: the semi-massive ore occurs in the core of the breccia surrounded by the disseminated ore, which grades outwards without changes in the silicate mineralogy to sulfide-free gabbronorite (Fig. 2). Minor chalcopyrite-rich veins also occur, cross-cutting both semi-massive and disseminated ore throughout the deposit.

*Figure 2.*

Semi-massive ore averages 21.1 wt. % S, 4.5 wt. % Ni, and 1.3 wt. % Cu (Piña et al. 2008). Ni/Cu ratios are commonly higher than 5, and Os, Ir, Ru and Rh are significantly more abundant when compared to the content of these metals in the disseminated ore. The high modal abundance of pyrrhotite, the predominance of pentlandite over chalcopyrite and the enrichment in Ni, Os, Ir, Ru and Rh and depletion in Cu, Au, Pt and Pd relative to disseminated ore indicate that the semi-massive ore represents MSS-enriched cumulates. In the disseminated ore, Cu (ave. 1.29 wt. %) typically predominates over Ni (ave. 0.72 wt. %). These sulfides are relatively enriched in Pd, Pt and Au in comparison with the semi-massive ore. The disseminated sulfides represent an original unfractionated sulfide liquid retained as droplets in the host gabbronorite (Piña et al. 2008).

Unmineralized mafic-ultramafic inclusions are concentrated preferentially but erratically within the semi-massive ore, but they also occur in the disseminated ore and even in sulfide-free gabbronorite. Observations by Piña et al. (2006) on the petrology, mineral chemistry and geochemistry of these inclusions are summarized here. Fragments comprise different cumulate-textured rock types: peridotite (dunite, harzburgite and werhlite), pyroxenite (orthopyroxenite and clinopyroxenite), gabbro (gabbro, hornblende gabbro and gabbronorite) and anorthosite. Gabbro (clinopyroxene + plagioclase) is by far the most abundant fragment-type. Xenoliths of calc-silicate hornfels, probably coming from the skarn formed along the north contact of the Aguablanca stock, are randomly distributed within the breccia. Fragments are commonly unmineralized, although some contain very minor disseminations interstitial to primary silicates or in association with secondary minerals such as epidote or actinolite. Minor chalcopyrite veinlets cut both fragments and host rocks. The primary silicate assemblage includes olivine (Fo91–Fo79), orthopyroxene (Mg no. 0.85–

0.73), clinopyroxene (Mg no. 0.93–0.62), plagioclase (An99–An38), amphibole (Mg no. 0.87–0.68) and phlogopite (Mg no. 0.89–0.64). The wide range of rock types and Mg numbers in the primary ferromagnesian silicates suggest magmatic differentiation processes from the parent melts, with the fragments representing different stages of cumulate formation. The ore-bearing breccia contains both semi-massive and disseminated sulfides in the gabbro matrix. Textures in the matrix vary between meso- and orthocumulate, and the rock-forming magmatic silicates are orthopyroxene (Mg no. 0.83–0.74), clinopyroxene (Mg no. 0.89–0.78), plagioclase (An50–An77), and intercumulus amphibole (Mg no. 0.86–0.70), phlogopite (0.84–0.69) and minor quartz. The gabbro in the matrix of the breccia is petrographically and chemically very similar to that of the unmineralized parts of the main Aguablanca intrusion and exhibits a similar differentiation trend, suggesting that the matrix of the ore-bearing breccia and the unmineralized rocks are products of the same magma. Based on the cumulate textures, the wide range of rock types from ultramafic to mafic, and Fe-enrichment trends in the primary ferromagnesian silicates, these fragments have previously been interpreted to be derived from different stages of cumulate formation of the same magma that produced the unmineralized portions of the intrusion. Previous models have attributed their origin to crystallisation in an underlying differentiating magma chamber (Piña et al. 2006).

### 3. Samples and methods

A suite of twelve samples was selected for detailed XRF mapping, representing a spectrum from silicate-matrix intrusion breccias with minor sulfide to sulfide-matrix breccias with >50% sulfide, all containing polymict assemblages of igneous autoliths from the intrusion, and in some cases containing probable country rock xenoliths. Samples were mostly collected from drill core within the main volume of semi-massive ore across into the flanking disseminated ores, supplemented by three samples from near the bottom of the open pit. Of these, 6 samples are illustrated in detail here, with scans of the additional samples presented as supplementary material.

The main technique employed in this study is desktop microbeam XRF mapping, using a Bruker Tornado instrument M4 Tornado™ instrument at the Commonwealth Scientific and Industrial Research Organization (CSIRO), Perth, equipped with a rhodium target X-ray tube operating at 50 kV and 500 nA without filters and an XFlash® silicon drift X-ray detector. Maps were created using a 40 µm spot size on a 40 µm raster with dwell times of 5–40 (most

commonly 10) ms per pixel. Further details of the method and the data visualization protocols are reported by Barnes et al. (2017). In addition, two samples were scanned at higher pixel resolution of 4  $\mu\text{m}$  using the Maia multi-detector array on the XFM beamline of the Australian Synchrotron (Ryan et al., 2014) using the Kirkpatrick Baez mirror microprobe end-station. This provides a monochromatic 2  $\mu\text{m}$  beam-spot size for energies in the range 4–20 keV. Equipped with the Maia 384 detector array, the XFM beamline can acquire data at 2  $\mu\text{m}$  resolution from 384 detectors simultaneously over areas of several square centimetres with count rates of  $\sim$  4–10 M/s, energy resolution of 300–400 eV. These spectra are then processed using the GeoPIXE software into maps of quantified element concentrations based on non-standardised correction of raw count data.

## 4. Results

This section describes the results of the element mapping for the chosen examples of sulfide-rich and sulfide-poor breccias. We use the non-genetic term “inclusion” rather than “clast”, and where context requires we refer to endogenously-derived igneous inclusions from the host intrusion as “autoliths” to distinguish them from “xenoliths” derived from outside the host intrusion.

### 4.1. Sulfide-rich sulfide matrix breccias with mafic-ultramafic clasts

#### 4.1.1. Sample AB-NA1

Sample AB-NA1 (Fig. 3, from the open pit) is a typical example of a sulfide-rich Aguablanca ore breccia containing inclusions of mafic and ultramafic rocks. Margins of the inclusions show a progression into “clouds” of individual crystals that become progressively dispersed into the sulfide matrix. This is a common feature in sulfide-matrix ore breccias from a number of localities, and we term them “soft-wall breccias” to distinguish this texture from e silicate inclusions that have sharp walls (at grain scale) against sulfide.

#### Figure 3 AB-NA1

The large inclusion on the bottom right of sample AB-NA1, as viewed in Fig. 3a, as well as the partially sampled inclusion on the top left, consists of anorthositic gabbro with a rind of pyroxenite between about 1 and 5 crystals thick, which closely resembles the soft-walled inclusions of pyroxenite in the lower left of the sample. A very distinctive feature of this sample, a feature that appears to be common to the pyroxenitic rocks at Aguablanca, is the presence of distinctive reverse and sometime oscillatory zoning with respect to the Cr content of euhedral clinopyroxene grains. Reverse zoning is present within a disaggregated pyroxene

crystals entirely surrounded by sulfide as well as in a small proportion of pyroxene crystals in the interior of the pyroxenite clasts (Fig. 3b, e). Zoned grains typically show complex concentric zoning, with the outermost rim being relatively Cr-poor (Fig. 4). The pyroxene assemblage also contains about 50% of orthopyroxene, commonly showing extensive alteration to talc, and in many cases showing mildly dendritic to hopper morphologies indicative of rapid crystallisation.

*Figure 4*

Sample AB-NA1 also contains another noteworthy feature. Pyroxene grains are not uniformly distributed through the sulfide matrix. They tend to be more highly concentrated within the composite pyrrhotite-pentlandite grains that represent the exsolution breakdown of original magmatic MSS grains (e.g. top half of Fig. 3d) relative to much lower proportions within chalcopyrite grains.

#### *4.1.2. Sample AB-SB2*

This sample, imaged by high-resolution synchrotron XFM (Fig. 5), consists of closely-packed gabbroinorite inclusions with interstitial sulfide patches that are choked with coarse, mainly euhedral plagioclase, orthopyroxene and clinopyroxene. The clinopyroxene and plagioclase in the inclusions have similar compositions to those in the dispersed grains in the sulfide matrix, but the latter are notably coarser and more euhedral. Orthopyroxene is more abundant in the sulfide matrix, where it shows a tendency to Mn enrichment in the rims (Fig. 5c). Zoning of Cr in pyroxene was not resolvable in this section, neither in the inclusions nor enclosed in the sulfide matrix. Plagioclase is partially replaced by sulfide (chalcopyrite, pyrrhotite and pentlandite in similar proportions to the matrix), and commonly shows a rim of biotite where enclosed in sulfide; in Fig. 5b it appears that the biotite defines the original rim of now slightly resorbed plagioclase. Similar rimming of plagioclase by biotite at sulfide-plagioclase contacts was noted at Voisey's Bay (Barnes et al., 2017), although it is much less consistently developed in the Aguablanca samples.

*Figure 5*

#### *4.1.3. Sample AB-RP1*

Sample AB-RP1 (Fig. 6) consists of very irregular, cusped inclusions of a high-Mg basaltic material showing fine, skeletal clinopyroxene grains closely resembling random pyroxene micro-spinifex in komatiitic basalts (Arndt et al., 2008). The fine intergrowth with sulfide, the presence of these textures suggestive of crystallisation from a previously superheated melt (Lofgren, 19080), and the distinctive cusped geometry of the clast margins suggest that this

sample is a melt-emulsion “breccia” formed as a physical mixture of molten silicate and sulfide magma. Such hybrid emulsion rock types have been described at silicate-sulfide contacts at Sudbury (Hawley, 1962) and in two examples of Western Australian komatiite-hosted ores: Moran shoot, Kambalda (Staude et al., 2016; Staude et al., 2017), and Silver Swan (Dowling et al., 2004).

*Figure 6.*

#### 4.1.4. Sample U160-01-2.7

Sample U160-01-2.7 (Figure 7) contains a disaggregating anorthosite clast and abundant subhedral clinopyroxene crystals showing open packing in a Cu-rich sulfide matrix. The anorthosite shows a mesocumulate texture, with interstitial clinopyroxene grains and distinct zoning of the plagioclase towards albitic outer rims. Sulfide penetrates along grain boundaries and microfractures within the anorthosite, as plagioclase crystals become detached into the sulfide matrix with apparent “jigsaw fit” morphology. The proportion of pyroxene to plagioclase increases further away from the anorthosite inclusion into the sulfide matrix.

## 4.2. Sulfide-poor silicate matrix breccias

### 4.2.1. Sample AGU84-79

This sulfide-poor breccia sample consists of a polymict assemblage of inclusions including fine-grained aluminous metapelite, fine Ca-rich calc-silicate probably representing metasomatised marble and anorthositic gabbro, within a pyroxenitic melagabbro matrix with “soft” margins against sulfide patches (Fig. 8). The matrix contains clinopyroxenes with the same style of reverse Cr zoning noted above, in this case clearly dispersed within the pyroxenitic gabbro away from contacts with sulfide. The sulfide component in this case contains a small proportion of late overgrown euhedral pyrite. The contact of the metapelite against gabbro is slightly diffuse at mm scale, with a partial rind of plagioclase while that against the sulfide shows a fine emulsion-dispersion texture at sub-mm scale. The calc-silicate xenolith has sharp contacts against both silicate and sulfide matrix, although there is a fine reaction rim marked by Fe-enrichment against the gabbroic matrix. This is interpreted as reaction of wollastonite from the calc-silicate with Fe and Mg from the gabbro to form augite. The more mafic metapelite clast has a marginal K-rich reaction rind reflecting growth of feldspar. There is no indication of Cr enrichment at clast margins, and no penetration of sulfide into the calc-silicate or central metapelite clast.

*Figure 8.*

#### 4.2.2. *Sample AGU84-137*

This sample (Fig. 9) contains a mixture of zoned calc-silicate xenolith inclusions, one of which is itself a fragmental rock, and a medium-grained gabbroic inclusion in the typical matrix of pyroxenitic melagabbro containing abundant secondary amphibole, with isolated 2-10 mm coherent patches of sulfide. Coarse 1 mm apatite grains are present within the matrix, in one case enclosed within sulfide. One of the calc-silicate inclusion shows a semi-continuous but very fine (~100 nm) rind of Cr enrichment and single-grain thick overgrowth of clinopyroxene in places, and overgrowth by plagioclase elsewhere. The gabbro inclusions contain a few phenocrysts of reverse-Cr-zoned clinopyroxene within an amphibole-plagioclase assemblage. Sulfide showing typical po-pn-cp magmatic mineralogy is developed within the matrix and the gabbro inclusion but not in the calc-silicate xenolith.

*Figure 9.*

## 5. Discussion

### 5.1. Summary of observations

Microbeam XRF mapping has revealed a number of distinctive features of the Aguablanca breccias that were not evident from previous conventional petrography.

1. A common feature of all the samples studied (including those not described here but illustrated in supplementary material) is that the matrix of the breccias is a bimodal mixture of a pyroxenite or pyroxene-phyrlic gabbro and sulfide, with variable degrees of disaggregation of pyroxenite (Fig. 3) or anorthosite (Fig. 7) along original grain boundaries accompanying infiltration by sulfide liquid. As the abundance of sulfide increases, the proportion of plagioclase in the remaining silicate matrix diminishes. In some cases (e.g. Fig. 3), the pyroxenitic gabbro itself forms disaggregating inclusions.
2. In sulfide-rich samples, silicate fragments and disaggregated pyroxene grains are preferentially enclosed in former MSS (now pyrrhotite-pentlandite) relative to chalcopyrite.
3. The pyroxenitic gabbro contains a population of distinctive euhedral clinopyroxene grains that show reverse zoning in Cr (Cr poor cores, Cr-rich rims). In many cases this zoning is oscillatory. Some gabbroic clasts also contain such grains, implying that they pre-date formation of the breccias. Identically zoned pyroxene grains of similar habit and size are observed entirely enclosed in sulfide around the edges of the inclusions. Significantly, the most Cr-rich zones of these pyroxenes are not located at

the outer contacts with sulfide, further arguing that this zonation is not the consequence of reaction with sulfide. This indicates that the “crystal clouds” surrounding the inclusions are derived by disaggregation of original pyroxene orthocumulate with preferential removal of an original interstitial silicate component.

4. The clasts show varying but generally very minor degrees of marginal chemical interaction where in contact with gabbroic matrix, evident as narrow (mm-scale) zones of enrichment of Fe (calc silicates), Cr (some calc silicates), and K (metapelites). These zones are restricted to the outer few mm at most.
5. None of the country rock clasts contain sulfides, which are restricted to interstitial or patchy net-textured domains within the pyroxenitic melagabbro matrix.

### 5.2. Origin of reverse-zoned pyroxenes

The phenomenon of reverse and oscillatory zoned pyroxenes (Fig. 4) in mineralized mafic-ultramafic conduit intrusions has been identified previously in the Ntaka Hill deposit in Tanzania (Barnes et al., 2016c). In this setting, the formation of reverse zoned pyroxenes is attributed to dynamic crystallisation and equilibration with carrier magma in mafic magma flowing through a conduit where active assimilation of the wall rock is taking place. Fluctuation in Cr content in pyroxene may be driven in part by changes in the Cr content of the magma, but more effectively by highly localized changes in redox state and silica activity that affect the partition coefficient of Cr into pyroxene (Campbell and Borley, 1974; Barnes, 1986).

An alternative mechanism that needs to be considered is whether reverse Cr zoning is the result of reaction of cumulus pyroxenes (and pre-existing mafic rock xenoliths) with sulfide liquid. This possibility is raised by the common presence of narrow zones of strong enrichment in chromite at sulfide-silicate contacts in komatiite-hosted deposits (Ewers et al., 1976; Barrett et al., 1977; Frost and Groves, 1989; Dowling et al., 2004; Fonseca et al., 2008; Staude et al., 2016; Staude et al., 2017). Two critical observations are relevant here. Firstly, in many cases including that documented in Fig. 4, the outermost zone of the zoned grains is actually Cr poor. Secondly, reverse zoned pyroxenes are also observed in the interior of pyroxenite matrix and inclusions away from contact with sulfide (Figs. 3, 9), while many pyroxene grains in contact with sulfide do not show marginal Cr enrichment. Furthermore, not all samples show this feature: there is no Cr zoning at all observed in the pyroxenes mapped in Fig. 5. This sample is particularly telling: pyroxenes in the inclusions in this sample are Cr-poor and show minor reverse zoning in Mn, features which are also present in

the pyroxenes enclosed in the surrounding sulfide (Fig 5d). Evidence from other deposits is that Cr is a very minor component in magmatic sulfide liquids; while chromite is found at contacts between molten sulfide and silicate in komatiite settings (e.g. Staude et al., 2017) the dominant oxide phase in mafic-hosted magmatic sulfide deposits is invariably magnetite, not chromite (e.g. Dare et al., 2014). We conclude that the zoning is a feature inherited from silicate cumulus processes, and that interaction with sulfide had minimal effect. Some very minor marginal enrichment in Cr in calc silicate clasts has been noted (Fig. 9) in a sulfide-poor breccia; we attribute this to reaction of the clast with silicate magma.

The significance of these zoning patterns from the point of view of the origin of the sulfide-matrix breccias is that the silicate component of the breccias is characteristically disaggregating along the original silicate grain boundaries of an orthocumulate precursor. The alternative possible interpretation, that the pyroxene crystals are growing from the sulfide liquid, or as a result of chemical exchange between the silicate and sulfide melts, is ruled out by the zoning evidence, and by the implausibility of crystallising a phase from a sulfide liquid that contains minimal concentrations of the essential components, Si and Mg. Coupled with the total absence of shear fabrics, grain size reduction, rotated inclusions, pressure shadows and within-grain deformation, this provides strong evidence that these are igneous and not *durchbewegung* tectonic breccias.

### 5.3. Interpretation of sulfide-matrix breccia textures

We propose the following sequence of events to account for the spectrum of observed textures, from sulfidic silicate-matrix intrusion breccias through to soft-clast sulfide matrix breccias at Aguablanca (Fig. 10).

*Figure 10.*

- 1) The early stages of the intrusion developed within successively opening tensional cracks within the Cherneca Fault zone (Tornos et al., 2005; Tornos et al., 2006; Pina et al., 2010). The disseminated ores formed as part of a cumulate sequence accreting inward from the sidewalls of the Aguablanca stock, as a result of accumulation of sulfide liquid droplets with cumulus plagioclase, orthopyroxene and clinopyroxene. The derivation of this sulfide cannot be inferred on current evidence, and may have been from above or below.
- 2) Emplacement of intrusion breccias by gravity flow of xenolith- and sulfide-rich “sludge” into the core of the intrusion, following accumulation of the surrounding disseminated ores. This process may have occurred during a late drain-back stage of

magma emplacement (Barnes et al., 2016b) as the magma flux through the intrusion network waned. The xenoliths could have been generated at the upper side walls and now-eroded roof of the host intrusion, as suggested by Barnes and Mungall (2018) for examples of sulfide-matrix breccias in dike-shaped intrusions. Alternatively, breccia accumulation may represent a stage where the accumulated load of xenoliths, phenocrysts and sulfide droplets in an ascending suspension increased to the point where the suspension was no longer buoyant relative to the country rocks, resulting in choking of the conduit neck. The resulting intrusion breccias consist of polymict assemblage of ultramafic, anorthositic and gabbroic autoliths and country-rock xenoliths in a matrix of gabbro and pyroxene orthocumulate (Figure 10A). Zoning in pyroxene grains is already present at this stage owing to a precursor history of crystallization from heterogeneous, variably contaminated magma in the conduit system, possibly due to similar processes to those proposed for the Ntaka Hill intrusion (Barnes et al., 2016c).

- 3) Sulfide percolation through the intra-clast pore space induces partial re-melting of pyroxene-plagioclase eutectic assemblages in the matrix and the autoliths. Infiltration of the sulfide melt displaces this relatively buoyant silicate melt component, which forms an upward counter-flow against the descending sulfide (Figure 10B). This results in the remaining silicate matrix component being enriched in pyroxene relative to the original gabbro assemblage. The pyroxenite rims around the gabbroic inclusions (Fig. 3) can be explained in either of two ways: firstly, by selective eutectic melting of plagioclase-pyroxene assemblages around the edge of the autoliths, leaving only pyroxene behind; secondly, by original embedding of the autoliths within a silicate matrix which itself was a pyroxene orthocumulate; the pyroxenite component may have formed part of the matrix as well as some of the clasts (Fig. 10). Much of the displaced silicate melt from both clasts and matrix “floats” out, in a process analogous to that inferred for patchy net textured ores, Voisey’s Bay breccias and inter-spinifex ores in komatiite-hosted deposits (Barnes et al., 2016a; Barnes et al., 2017a).
- 4) Partial melting of silicate clasts and pyroxenite matrix as a result of sulfide liquid penetration (e.g. Fig. 3C, Fig. 4) causes disaggregation along original crystal boundaries. Open crystal frameworks develop within sulfide matrix, and complexly-zoned cumulus pyroxene grains become isolated within the sulfide melt (Figure 10C).

- 5) Initial crystallisation of sulfide liquid forms large grains of MSS that trap silicate grains and prevent them from floating up through sulfide liquid; these become preserved as frameworks of (often zoned) pyroxene crystals within pyrrhotite/pentlandite aggregates (Fig. 3D, Fig. 10E). This requires that the sulfide percolation process takes place within the melting range of the sulfide liquid, i.e. below 1100°C.
- 6) MSS crystallisation results in formation of a residual Cu-rich sulfide liquid. Percolation of this residual liquid continues, leaving behind a relatively Cu-poor, Ni-enriched MSS component, accounting for the MSS-cumulus enriched character of the semi-massive and breccia ores relative to the original bulk sulfide liquid as represented by the disseminated ores (Pina et al., 2010).

The very sharp contacts of the calc-silicate xenoliths, presumably metasomatised carbonate skarn clasts, gives us some insight into the mechanism of xenolith incorporation into magmas. The melting point of calcite is 1339°C and that of wollastonite 1540°C, indicating that calc-silicate rich rocks are incapable of melting in mafic magmas. Hence, they would be incorporated into magma by a process of dissolution, which is limited by the relatively slow process of chemical diffusion at a compositional boundary layer (Kerr, 1994; Kerr, 1995). The sharp boundaries of the xenoliths are a consequence of this control: only the outer few microns of the xenoliths are interacting with the magma, and hence the boundaries are sharp compared to those of xenoliths with lower melting points where melting is controlled by the much more rapid processes of partial melting.

## 6. Conclusions

From the foregoing arguments and observations, we conclude that the sulfide matrix breccias at Aguablanca, like those previously documented at Voisey's Bay (Barnes et al., 2017a), are the result of sulfide liquid infiltration into pre-existing, probably still partially molten, silicate-matrix intrusion breccias. These intrusion breccias may have developed by a number of mechanisms. Following the model for ore formation in trans-crustal sill-dyke complexes proposed by Barnes et al. (2016b), they may have formed as a result of downward gravity flows into the neck of the funnel-shaped Aguablanca intrusion during a period of back-flow, at the waning stage of the final magmatic episode in a long-lived conduit system, following the earlier accumulation of gabbroic cumulates with disseminated sulfides inwards from the

margins of the intrusion. These gravity flows may have incorporated sulfide liquid along with silicate magma and a “sludge” of variably digested xenoliths, or the sulfide liquid may have been added later as a result of downward flow of gravitationally unstable pools of sulfide liquid originally deposited higher in the system.

We offer the sulfide infiltration mechanism as an alternative to previous proposals (Tornos et al., 2006; Pina et al., 2010) that the breccias are the result of a process of upward tectonically-driven seismic pumping, forcing initially segregated sulfide liquid pools up from originally deeper deposit sites, a process which is physically implausible owing to the high density and very low viscosity of sulfide liquids (Saumur et al., 2015; Robertson et al., 2016; Saumur and Cruden, 2017). Sulfide liquid droplets can be entrained and transported in silicate magmas in any direction at low concentrations, owing to their propensity to break up into finer droplets during transport (Robertson et al., 2016). In the absence of isotopic evidence for a deep source, and given that the overlying roof rocks have been eroded away, we cannot therefore draw any conclusions about the ultimate direction of derivation of the sulfides. Further detailed investigation of S isotopes in the Aguablanca ores and potential S-supplying host rocks will be needed to further elucidate the source and overall transport direction of the sulfide, but the breccias provide evidence that the final stage of sulfide emplacement involved downward percolation. The most significant conclusion is that the Aguablanca ore breccias, like those at Voisey’s Bay, formed by essentially passive in-situ processes, and there is no necessity to invoke high-energy processes analogous to hydrothermal explosion breccias, or tectonic processes such as seismic pumping. The model presented here may well be applicable to other deposits where sulfide matrix breccias appear to develop late within the crystallisation history, and may be a marker for multistage magma flow in vertically extensive sill-dyke complexes.

### **Acknowledgments**

We thank Lundin Mining for access to samples and for hosting a mine visit. Nick Arndt, and Steve Beresford loaned some excellent samples. The synchrotron X-ray fluorescence maps were collected on the X-ray fluorescence microscopy beam line at the Australian Synchrotron, Clayton, Victoria, Australia. We acknowledge financial support for this facility from the Science and Industry Endowment Fund (SIEF), and the assistance of David Paterson and Chris Ryan with data collection and processing. We thank Valentina Taranovic for

comments on an early draft, and Jim Mungall and an anonymous reviewer for detailed reviews.

*Supplementary material:*

*PDF file containing annotated images of all 12 samples imaged in this study. Supp-Aguablanca-breccias.pdf*

## References

- Arcuri, T., Ripley, E. M., and Hauck, S. A., 1998, Sulfur and oxygen isotope studies of the interaction between pelitic xenoliths and basaltic magma at the Babbitt and Serpentine Cu-Ni deposits, Duluth Complex, Minnesota: *Economic Geology and the Bulletin of the Society of Economic Geologists*, v. 93, p. 1063-1075.  
doi:<http://dx.doi.org/10.2113/gsecongeo.93.7.1063>
- Arndt, N. T., Leshner, C. M., and Barnes, S. J., 2008, *Komatiite*: Cambridge, Cambridge University Press, 467 p.
- Barnes, S. J., 1986, The distribution of chromium among orthopyroxene, spinel and silicate liquid at atmospheric pressure: *Geochimica et Cosmochimica Acta*, v. 50, p. 1889-1909.
- Barnes S.J., Mungall J.E., 2018, Blade shaped dykes and nickel sulfide deposits: a model for the emplacement of ore-bearing small intrusions. *Economic Geology*, in press.
- Barnes, S. J., Beresford, S. W., and Le Vaillant, M., 2016a, Interspinifex Ni sulfide ore from the Coronet Shoot, Kambalda: characterisation using microbeam XRF mapping and 3D X-ray computed tomography: *Economic Geology*, v. 111, p. 1509-1517.  
doi:[10.2113/econgeo.111.6.1509](https://doi.org/10.2113/econgeo.111.6.1509)
- Barnes, S. J., Cruden, A. R., Arndt, N. T., and Saumur, B. M., 2016b, The mineral system approach applied to magmatic Ni-Cu-PGE sulphide deposits: *Ore Geology Reviews*, v. 76, p. 296-316. doi:[10.1016/j.oregeorev.2015.06.012](https://doi.org/10.1016/j.oregeorev.2015.06.012)
- Barnes, S. J., Le Vaillant, M., and Lightfoot, P. C., 2017a, Textural development in sulfide-matrix ore breccias and associated rocks in the Voisey's Bay Ni-Cu-Co deposit, Labrador, Canada: *Ore Geology Reviews*, v. in press.  
doi:[10.1016/j.oregeorev.2017.03.019](https://doi.org/10.1016/j.oregeorev.2017.03.019)
- Barnes, S. J., Mole, D. R., Le Vaillant, M., Campbell, M., Verrall, M., Roberts, M., and Evans, N. J., 2016c, Poikilitic textures, heteradcumulates and zoned orthopyroxenes in the Ntaka Ultramafic Complex, Tanzania: implications for crystallisation mechanisms of oikocrysts: *Journal of Petrology*, v. 57, p. 1171-1198.  
doi:[10.1093/petrology/egw036](https://doi.org/10.1093/petrology/egw036)
- Barnes, S. J., Mungall, J. E., Le Vaillant, M., Godel, B., Leshner, C. M., Holwell, D. A., Lightfoot, P. C., Krivolutsкая, N. A., and Wei, B., 2017b, Sulfide-silicate textures in magmatic Ni-Cu-PGE sulfide ore deposits: Disseminated and net-textured ores.: *American Mineralogist*, v. 102, p. 473-506. doi:[10.2138/am-2017-5754](https://doi.org/10.2138/am-2017-5754)
- Barrett, F. M., Binns, R. A., and Groves, D. I., 1977, Structural history and metamorphic modification of Archaean volcanic-type nickel deposits: *Economic Geology*, v. 72, p. 1195-1223.

- Campbell, I. H., and Borley, G. D., 1974, The geochemistry of pyroxenes from the Lower Layered Series of the Jimberlana Intrusion, Western Australia: *Contributions to Mineralogy and Petrology*, v. 47, p. 281-297.
- Casquet, C., 1980, Fenómenos de endomorfismo, metamorfismo y metasomatismo en los mármoles de la Rivera de Cala (Sierra Morena), Universidad Complutense de Madrid, 295 p.
- Casquet, C., Galindo, C., Tornos, F., Velasco, F., and Canales, A., 2001, The Aguablanca Cu-Ni ore deposit (Extremadura, Spain), a case of synorogenic orthomagmatic mineralization: age and isotope composition of magmas (Sr, Nd) and ore (S). *Ore Geology Reviews*, v. 18, p. 237-250.
- Dare S.A.S., Barnes S.-J., Beaudoin G., Meric J., Boutroy E., Potvin-Doucet C., 2014, Trace elements in magnetite as petrogenetic indicators. *Mineralium Deposita*, 49, 785-96:
- De Angelis, M., Hoyle, M. W. H., Peters, W. S., and Wightman, D., 1987, The nickel-copper deposit at Radio Hill, Karratha, Western Australia: *Australasian Institute Mining Metallurgy Bulletin and Proceedings*, v. 292, p. 61-74.
- Dowling, S. E., Barnes, S. J., Hill, R. E. T., and Hicks, J., 2004, Komatiites and Nickel Sulfide Ores of the Black Swan area, Yilgarn Craton, Western Australia. 2. Geology and Genesis of the Orebodies.: *Mineralium Deposita*, v. 39, p. 707-728.
- Evans-Lamswood, D. M., Butt, D. P., Jackson, R. S., Lee, D. V., Muggridge, M. G., Wheeler, R. I., and Wilton, D. H. C., 2000, Physical controls associated with the distribution of sulfides in the Voisey's Bay Ni-Cu-Co deposit, Labrador: *Economic geology and the Bulletin Of the Society Of Economic Geologists*, v. 95, p. 749.
- Ewers, W. E., Graham, J., Hudson, D. R., and Rolls, J. M., 1976, Crystallisation of chromite from nickel-iron sulphide melts: *Contributions to Mineralogy and Petrology*, v. 54, p. 61-64.
- Fonseca, R. O. C., Campbell, I. H., O'Neill, H. S. C., and Fitzgerald, J. D., 2008, Oxygen solubility and speciation in sulphide-rich mattes: *Geochimica et Cosmochimica Acta*, v. 72, p. 2619-2635.
- Frost, K. M., and Groves, D. I., 1989, Magmatic contacts between immiscible sulfide and komatiitic melts; implications for genesis of Kambalda sulfide ores: *Economic Geology*, v. 84, p. 1697-1704.
- Hawley, J., 1962, The Sudbury ores, their mineralogy and origin; Part 1, The geological setting, : *Canadian Mineralogist*, v. 7, p. 1-29.
- Hicks, J., Barnes, S. J., Le Vaillant, M., and Mole, D., 2017, Savannah nickel sulfide deposits, in Phillips, N., ed., *Australian Ore Deposits Monograph*: Melbourne, Australian Institute of Mining and Metallurgy, p. 435-440.
- Kerr, R. C., 1994, Dissolving driven by vigorous compositional convection: *Journal of Fluid Mechanics*, v. 280, p. 287-302.
- Kerr, R. C., 1995, Convective crystal dissolution: *Contributions to Mineralogy and Petrology*, v. 121, p. 237-246. doi:10.1007/BF02688239
- Leshner, C., 2017, Roles of residues/skarns, xenoliths, xenocrysts, xenomelts, and xenovolatiles in the genesis, transport, and localization of magmatic Fe-Ni-Cu-PGE sulfides and chromite.: *Ore Geology Reviews*, v. in press. doi:10.1016/j.oregeorev.2017.08.008

- Li, C., and Naldrett, 2000, Melting reactions of gneissic inclusions with enclosing magma at Voisey's Bay, Labrador, Canada; implications with respect to ore genesis: *Economic geology and the bulletin of the Society of Economic Geologists*, v. 95, p. 801-814.
- Lightfoot, P. C., 2016, *Nickel Sulfide Ores and Impact Melts*, Elsevier, 680 p.
- Lightfoot, P. C., and Farrow, C. E. G., 2002, Geology, geochemistry, and mineralogy of the Worthington offset dike: A genetic model for offset dike mineralization in the Sudbury Igneous Complex: *Economic Geology and the Bulletin of the Society of Economic Geologists*, v. 97, p. 1419- 1446.
- Lightfoot, P. C., Keays, R. R., Evans-Lamswood, D., and Wheeler, R., 2012, S saturation history of Nain plutonic suite mafic intrusions; origin of the Voisey's Bay Ni-Cu-Co sulfide deposit, Labrador, Canada: *Mineralium Deposita*, v. 47, p. 23-50. doi:<http://dx.doi.org/10.1007/s00126-011-0347-6>
- Lightfoot, P. C., Keays, R. R., Morrison, G. G., Bite, A., and Farrell, K. P., 1997, Geologic and geochemical relationships between the contact sublayer, inclusions, and the main mass of the Sudbury Igneous Complex; a case study of the Whistle Mine Embayment: *Economic Geology and the Bulletin of the Society of Economic Geologists*, v. 92, p. 647-673. doi:<http://dx.doi.org/10.2113/gsecongeo.92.6.647>
- Lightfoot, P. C., Stewart, R., Gribbin, G., and Mooney, S. J., 2017, Relative contribution of magmatic and post-magmatic processes in the genesis of the Thompson Mine Ni-Co sulfide ores, Manitoba, Canada: *Ore Geology Reviews*, v. 83, p. 258-286.
- Lofgren G. 1980, Experimental studies on the dynamic crystallization of silicate melts. In: Hargraves RB, editor. *Physics of Magmatic Processes*. Princeton: Princeton University Press; p. 487-551
- Makkonen, H. V., 2015, Nickel deposits of the 1.88 Ga Kotalahti and Vammala Belts, *in* Maier, W. D., Lahtinen, R., and O' Brien, H., eds., *Mineral Deposits of Finland*, Elsevier, p. 253-287.
- Mariga, J., Ripley, E. M., and Li, C., 2006, Petrologic evolution of gneissic xenoliths in the Voisey's Bay Intrusion, Labrador, Canada: *Mineralogy, reactions, partial melting, and mechanisms of mass transfer: Geochemistry, Geophysics, Geosystems*, v. 7. doi:10.1029/2005GC001184
- Marshall, B., and Gilligan, L. B., 1989, Durchbewegung structure, pircementcusps and piercement veins in massive sulfide deposits: formation and interpretation: *Economic Geology*, v. 84, p. 2311-2319.
- Ortega, L., Lunar, R., Garcia-Palomero, F., Moreno, T., Martin-Estrevez, J. R., Prichard, H. M., and Fisher, P. C., 2004, The Aguablanca Ni-Cu-Pge Deposit, Southwestern Iberia: Magmatic Ore-Forming Processes and Retrograde Evolution: *Canadian Mineralogist*, v. 42, p. 325-350.
- Piña, R., Lunar, R., Ortega, L., Gervilla, F., Alapieti, T., and Martinez, C., 2006, Petrology and Geochemistry of Mafic-Ultramafic Fragments From the Aguablanca Ni-Cu Ore Breccia, Southwest Spain: *Economic Geology*, v. 101, p. 865-881.
- Pina, R., Romeo, I., Ortega, L., Lunar, R., Capote, R., Gervilla, F., Tejero, R., and Quesada, C., 2010, Origin and emplacement of the Aguablanca magmatic Ni-Cu-(PGE) sulfide deposit, SW Iberia; a multidisciplinary approach: *Geological Society of America Bulletin*, v. 122, p. 915-925. doi:<http://dx.doi.org/10.1130/B30046.1>

- Ripley, E. M., and Alawi, J. A., 1988, Petrogenesis of pelitic xenoliths at the Babbitt Cu-Ni deposit, Duluth Complex, Minnesota, U.S.A: *Lithos*, v. 21, p. 143-159.  
doi:[http://dx.doi.org/10.1016/0024-4937\(88\)90017-5](http://dx.doi.org/10.1016/0024-4937(88)90017-5)
- Robertson, J. C., Barnes, S. J., and Le Vaillant, M., 2016, Dynamics of magmatic sulphide droplets during transport in silicate melts and implications for magmatic sulphide ore formation: *Journal of Petrology*, v. 56, p. 2445-2472. doi:10.1093/petrology/egv078
- Romeo, I., Capote, R., and Lunar, R., 2007, Crystallographic preferred orientations and microstructure of a Variscan marble mylonite in the Ossa-Morena Zone (SW Iberia): *Journal of Structural Geology*, v. 29, p. 1353-1368.
- Romeo, I., Lunar, R., Capote, R., Quesada, C., Dunning, G. R., Piña, R., and Ortega, L., 2006, U/Pb age constraints on Variscan Magmatism and Ni-Cu-PGE metallogeny in the Ossa-Morena Zone (SW Iberia). *Journal of the Geological Society: Journal of the Geological Society*, v. 163, p. 837-846.
- Romeo, I., Tejero, R., Capote, R., and Lunar, R., 2008, 3-D gravity modelling of the Aguablanca Stock, tectonic control and emplacement of a Variscan gabbro-norite bearing a Ni-Cu-PGE ore, SW Iberia: *Geological Magazine*, v. 145, p. 345-359.
- Ryan, C. G., Siddons, D. P., Kirkham, R., Li, Z. Y., de Jonge, M. D., Paterson, D. J., Kuczewski, A., Howard, D. L., Dunn, P. A., Falkenberg, G., U, Boesenberg, U., De Geronimo, G., Fisher, L. A., Halfpenny, A., Lintern, M. J., Lombi, E., Dyl, K. A., Jensen, M., Moorhead, G. F., Cleverley, J. S., Hough, R. M., Godel, B., Barnes, S. J., James, S. A., Spiers, K. M., Alfeld, M., Wellenreuther, G., Vukmanovic, Z., and Borg, S., 2014, Maia X-ray fluorescence imaging: Capturing detail in complex natural samples, *Journal of Physics: Conference Series*, 499, p. 012002.
- Saumur, B. M., and Cruden, A. R., 2017, Ingress of magmatic Ni-Cu sulphide liquid into surrounding brittle rocks: physical & structural controls: *Ore Geology Reviews*, v. online. doi:<http://dx.doi.org/10.1016/j.oregeorev.2017.06.009>
- Saumur, B. M., Cruden, A. R., and Boutelier, D., 2015, Sulfide Liquid Entrainment by Silicate Magma: Implications for the Dynamics and Petrogenesis of Magmatic Sulfide Deposits: *Journal of Petrology*, v. 56, p. 2473-2490.
- Schäfer, H., Gebauer, D., Nägler, T., and Eguiluz, L., 1993, Conventional and ion-microprobe U-Pb dating of detrital zircons of the Tentudia Group (Serie Negra, SW Spain): implications for zircon systematics, stratigraphy, tectonics and the Precambrian/Cambrian boundary: *Contribution to Mineralogy and Petrology*, v. 113, p. 289-299.
- Seat, Z., Beresford, S. W., Grguric, B. A., Waugh, R. S., Hronsky, J. M. A., Gee, M. A. M., Groves, D. I., and Mathison, C. I., 2007, Architecture and emplacement of the Nebo-Babel gabbro-norite-hosted magmatic Ni-Cu-PGE sulphide deposit, West Musgrave, Western Australia: *Mineralium Deposita*, v. 42, p. 551-581.
- Staude, S., Barnes, S. J., and Le Vaillant, M., 2016, Evidence of lateral thermomechanical erosion of basalt by Fe-Ni-Cu sulfide melt at Kambalda, Western Australia: *Geology*, v. 12, p. 1047-1050. doi:10.1130/G37977.1
- Staude, S., Barnes, S. J., and Le Vaillant, M., 2017, Thermomechanical excavation of ore-hosting embayments beneath komatiite lava channels: textural evidence from the Moran deposit, Kambalda, Western Australia: *Ore Geology Reviews*, v. online. doi:10.1016/j.oregeorev.2017.05.001

- Tornos, F., Casquet, C., Galindo, C., Velasco, F., and Canales, A., 2001, A new style of Ni-Cu mineralization related to magmatic breccia pipes in a transpressional magmatic arc, Aguablanca, Spain: *Mineralium Deposita*, v. 36, p. 700-706.
- Tornos, F., Casquet, C., and Relvas, J., 2005, Transpressional Tectonics, Lower Crust Decoupling and Intrusion of Deep Mafic Sills: a Model for the Unusual Metallogenesis of Sw Iberia: *Ore Geology Reviews*, v. 27, p. 133-163.
- Tornos, F., Galindo, C., Casquet, C., Pevida, L. R., Martinez, C., Martinez, E., Velasco, F., and Iriondo, A., 2006, The Aguablanca Ni-(Cu) sulfide deposit, SW Spain; geologic and geochemical controls and the relationship with a midcrustal layered mafic complex: *Mineralium Deposita*, v. 41, p. 737-769.  
doi:<http://dx.doi.org/10.1007/s00126-006-0090-6>
- Velasco, F., 1976, *Mineralogía y metalogenia de las skarns de Santa Olalla (Huelva)*, Universidad del País Vasco, Spain, 290 p.

### Figure captions

Figure 1. A, geological map of the Aguablanca Intrusion (modified from Pina et al., 2010); B, 3D deep structure based on gravity inversion after Romeo et al. (2008).

Figure 2. Detailed geology (lithologies and mineralization) of the sulfide-bearing Aguablanca stock at the 450 level as interpreted by drill cores showing the disposition of ore-types. The section A-A' shows the vertical disposition of the ore-bearing breccia with the semi-massive ores preferentially located in the inner part surrounded by disseminated ores. The contour of the open-pit is shown. Modified from Piña et al. (2010).

Figure 3. Sample AB-NA1. a, incident light on polished slab, Anorth=anorthositic gabbro, Pxnite = pyroxenite. b-e, Tornado false-colour 3 element maps from microbeam XRF mapping (hereafter XFM maps). Assignment of elements to channels (red, green, blue) indicated on color triangles on each image. b, whole slab, S-Cr-Al, sulfides show up red. c, Cr-Si-Al – plagioclase in turquoise-blue shades, pyroxene orange (Cr-rich) to green; reverse Cr-zoned pyroxenes highlighted (arrows); note pyroxenite rind around anorthositic gabbro clast, lower right. d, e, same field of view, Ni-S-Cu and Cr-Fe-Si respectively; note cluster of disaggregated pyroxene grains enclosed in pyrrhotite (Po, top centre) compared with adjacent inclusion-poor chalcopyrite (Ccp). Cr-zoned pyroxenes arrowed.

Figure 4. Sample AB-NA1, high-resolution synchrotron XFM (Cr, Fe, Ca) map of polished thin section corresponding to lower left corner of Figure 3c. Note strong oscillatory and reversed zoning of Cr in cpx, relatively weak similar zoning in opx grains, both in sulfide matrix (green). Inset shows semi-quantitative profile of Cr content across line A-A', values obtained from GeoPixa software with calibration based on microprobe-XFM comparison by (Barnes et al., 2016c).

Figure 5. Sample ABSB-2, polished thin section. a, transmitted light photomicrograph showing sulfide (black), margins of gabbro and gabbro clasts, “film” of biotite (Bt) around rim of partially replaced plagioclase grain; b, enlargement of plagioclase with biotite “film”; c,d, and e same field of view as a, c is phase map made by thresholding element maps; d and e, high-resolution synchrotron XFM maps, d is Mn-Cr-Sr (note slight reverse zoning in Mn in opx), e is Ni-Cu-Fe, showing well developed loop texture (pentlandite around pyrrhotite grain boundaries) within sulfides interstitial to silicate mineral inclusions. Sulfide replacement of plagioclase (arrowed) is predominantly chalcopyrite.

Figure 6. sample AB-RP1, a-c same field of view of semi-polished drill core slab, incident light (a) and Tornado XFM maps (b, c) – clasts are fine-grained mafic Mg-rich dolerite showing micro-dendritic cpx indicative of complete melting under superheated conditions. Cuspate silicate-sulfide boundaries are characteristic of two-liquid melt emulsion texture.

Figure 7. Sample U160-01-2.7, cut drill core slab, incident light (a), Tornado XFM false-colour map (b) and (c) phase map made by thresholding element maps. Anorthosite clast in upper right shows jigsaw-fit disaggregation into single grains and grain aggregates of zoned plagioclase (lower Ca in rims shown by transition from pink to blue to turquoise colours in b) within a sulfide matrix containing a loosely packed aggregate of mainly euhedral clinopyroxene (cpx) crystals.

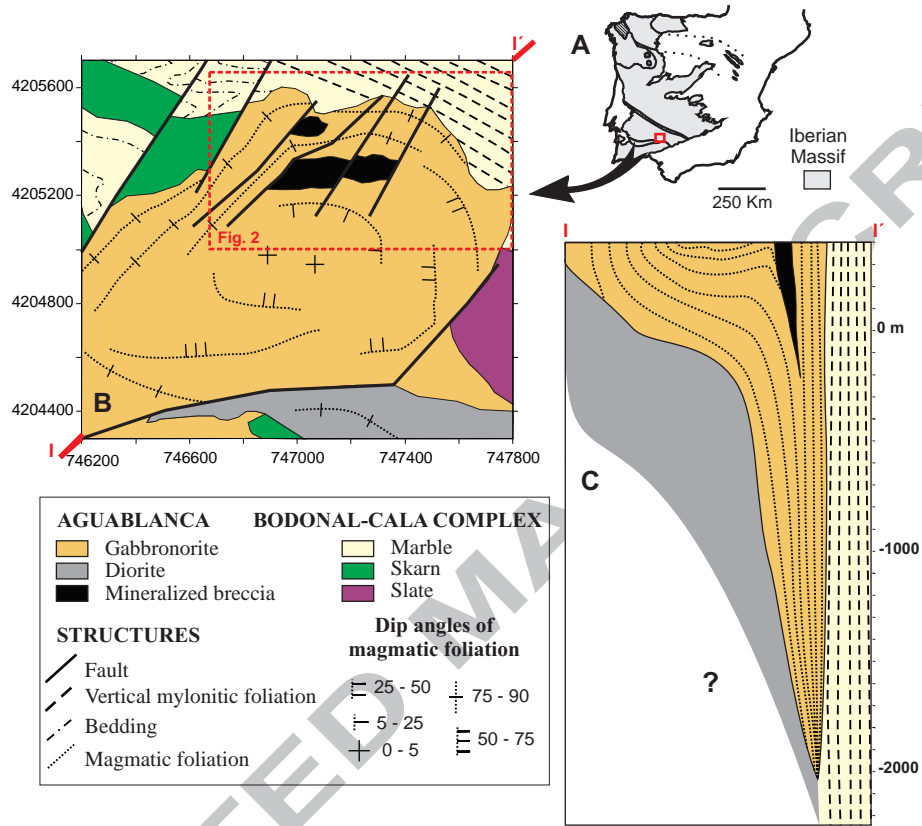
Figure 8. Sample AGU84-79, cut drill core slab, incident light (a) and Tornado XFM maps (b-f) showing a polymict dominantly silicate-matrix intrusion breccia with incipient invasion by sulfide (Sulf). Matrix is a variably pyroxene-enriched gabbro, clasts are a mixture of fine grained hornfelsed country rock types including K-rich and K-poor metapelite and wollastonite-rich calc-silicate skarn rock (calc sill). Inset shows detail of reverse Cr zoning in cpx grains in the gabbro matrix.

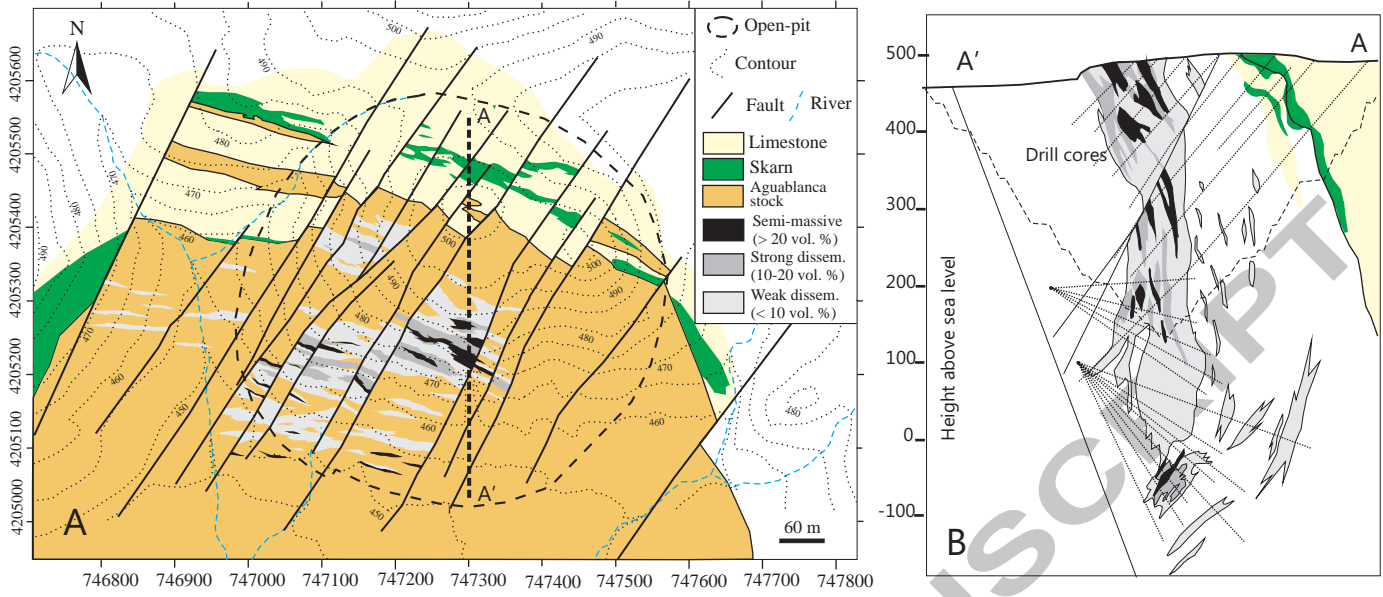
Figure 9. Sample AGU84-79, cut drill core slab, incident light (a) and Tornado XFM maps (b-f) showing a polymict dominantly silicate-matrix intrusion breccia with incipient invasion by sulfide (Sulf), similar to Figure 6 but with additional features: fine grained gabbroic clast with phenocryst of Cr-zone cpx (c, arrowed); very fine rind of Cr enrichment in the central calc-silicate clast, which is itself a breccia; very sharp (dissolution) boundaries on calc-silicate clasts.

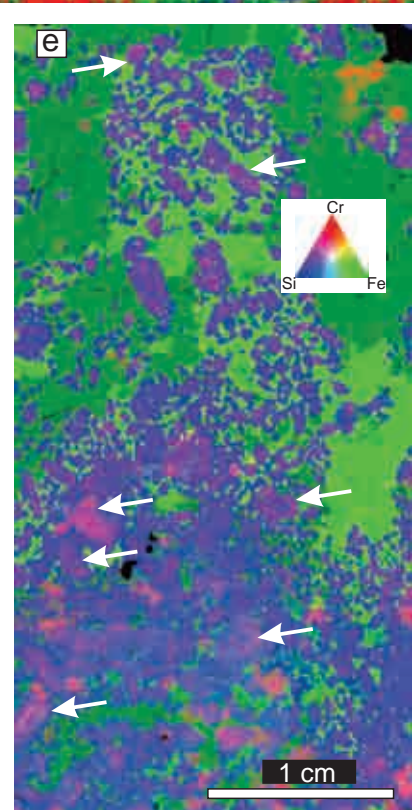
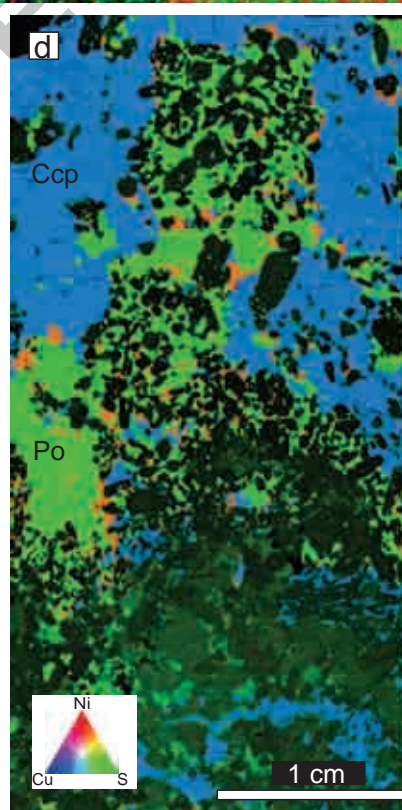
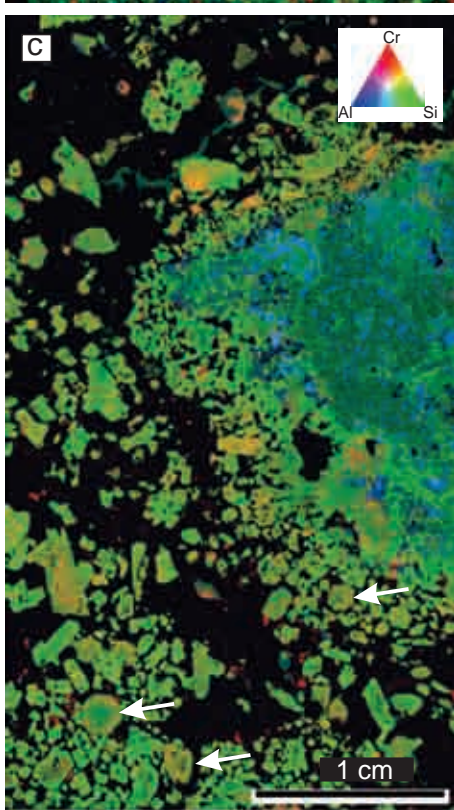
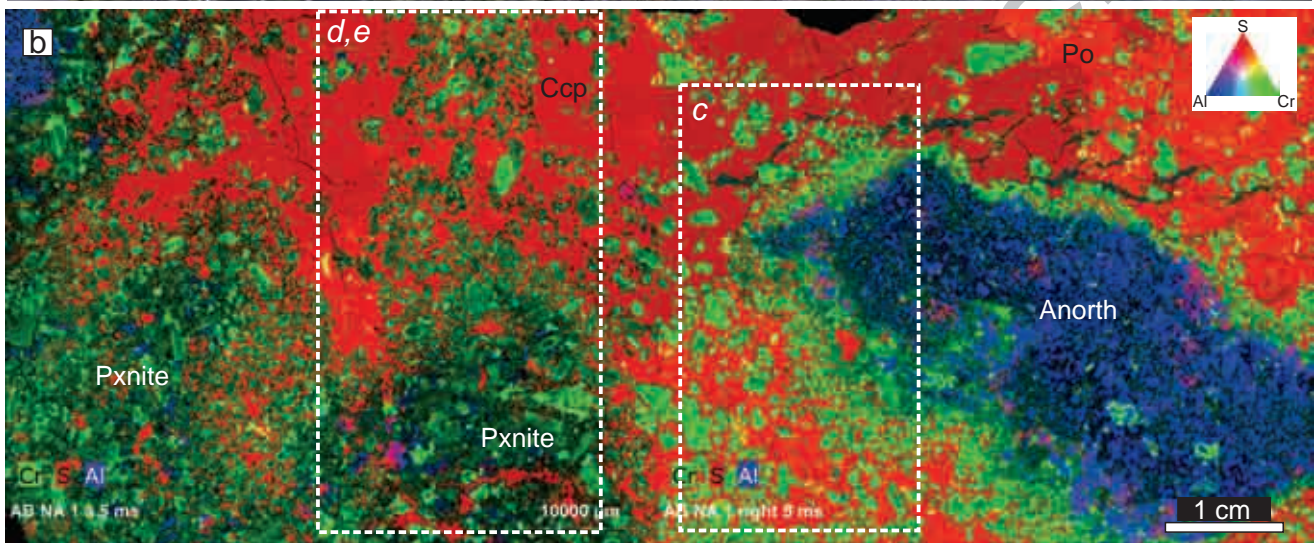
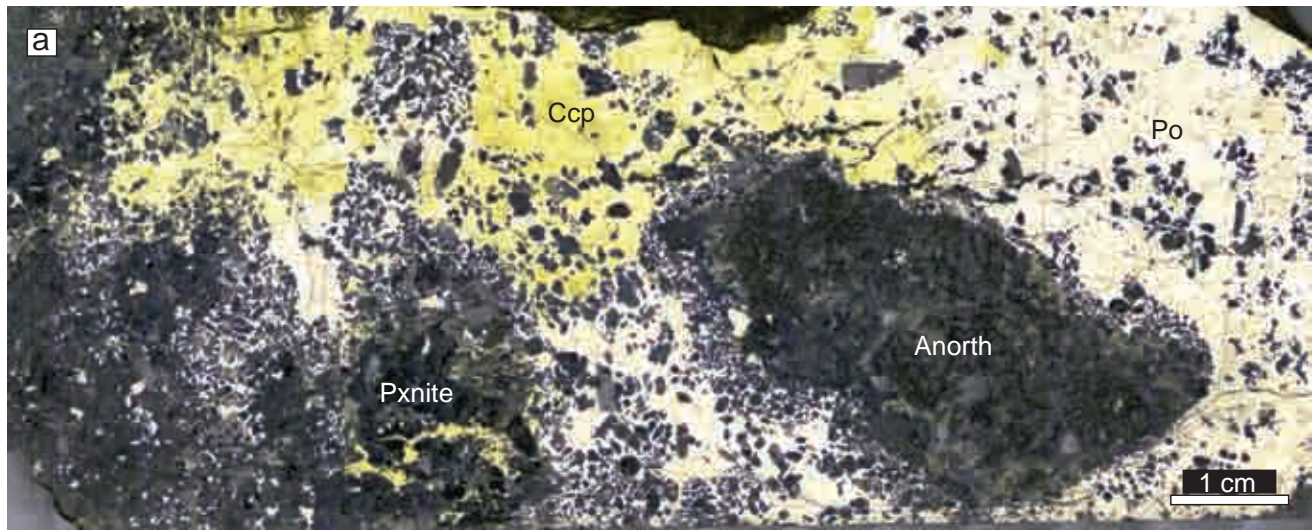
Figure 10. Cartoon showing model for development of sulfide-matrix breccias at Aguablanca. a), breccia consisting of polymict assemblage of ultramafic, anorthositic, gabbroic and country-rock clasts in matrix of partially solidified pyroxenitic melagabbro. b), sulfide percolation through intraclast pore space – displaces silicate melt component, partially melts pyroxene-plagioclase eutectic assemblages in matrix and clast margins, displaced silicate melt and some pyroxene “floats” out. c), initial crystallisation of sulfide liquid forms large grains of MSS that trap silicate grains and prevent them from floating up through sulfide liquid; these become preserved as frameworks of (often zoned) pyroxene crystals within pyrrhotite/pentlandite aggregates (inset e, Fig. 3d,e). d), ongoing infiltration and fractional crystallisation of sulfide melt, drainage of residual Cu-rich liquid, accompanied by upward

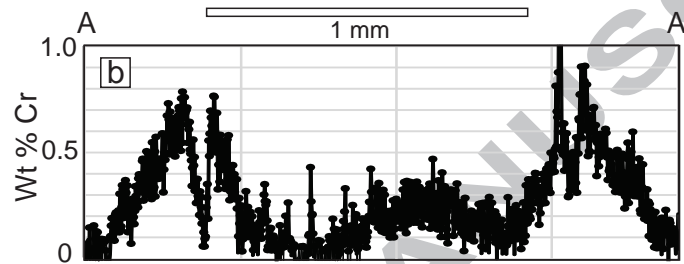
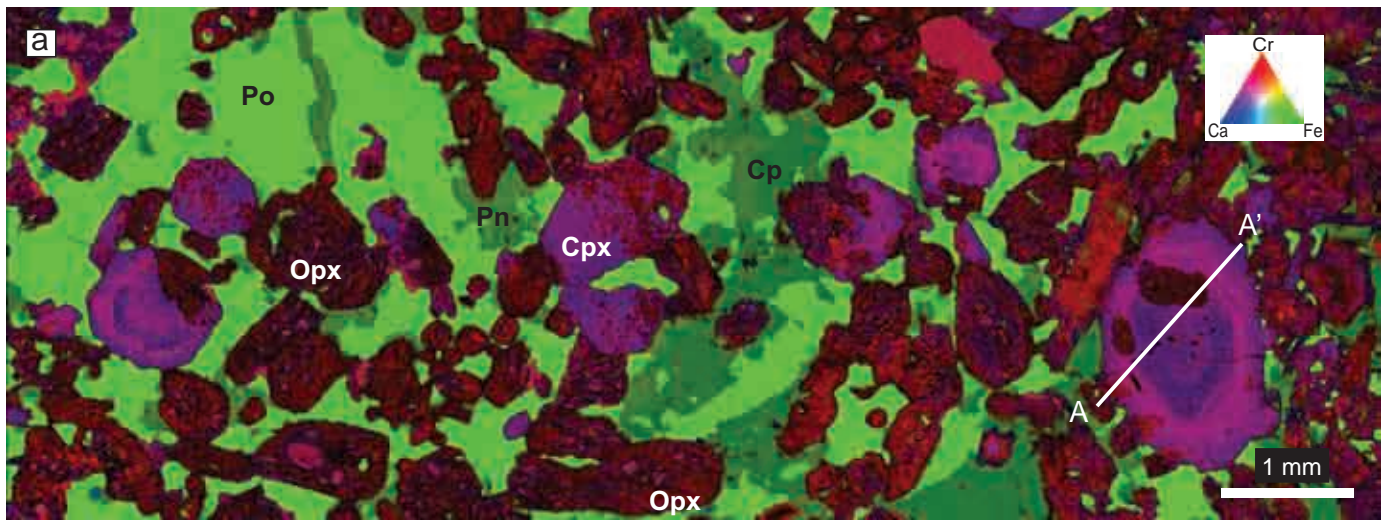
displacement of remaining silicate melt and pyroxene grains not enclosed in solid MSS. Pore space becomes flooded by Cu-rich residual sulfide melt. Inset e), detail of figure 2 showing pyroxene grains (black) enclosed within po+pn (original MSS, green+orange).

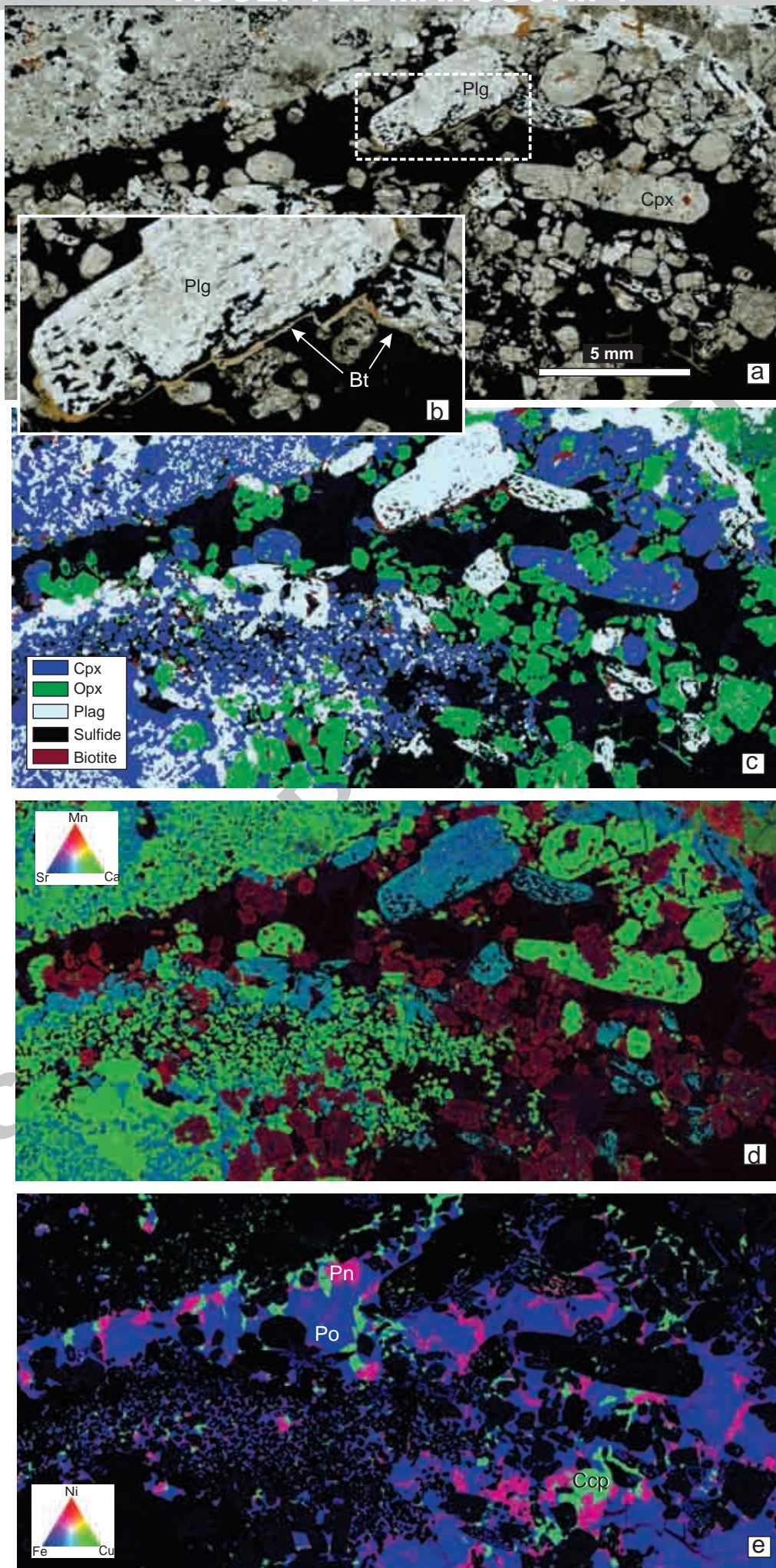
ACCEPTED MANUSCRIPT

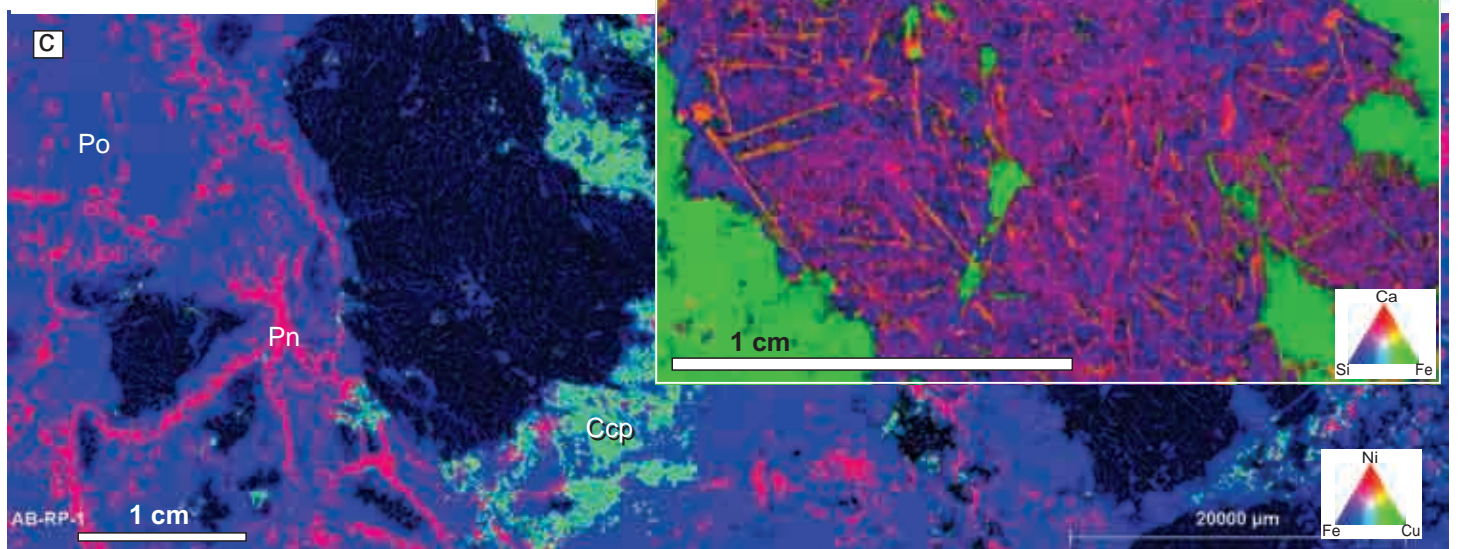
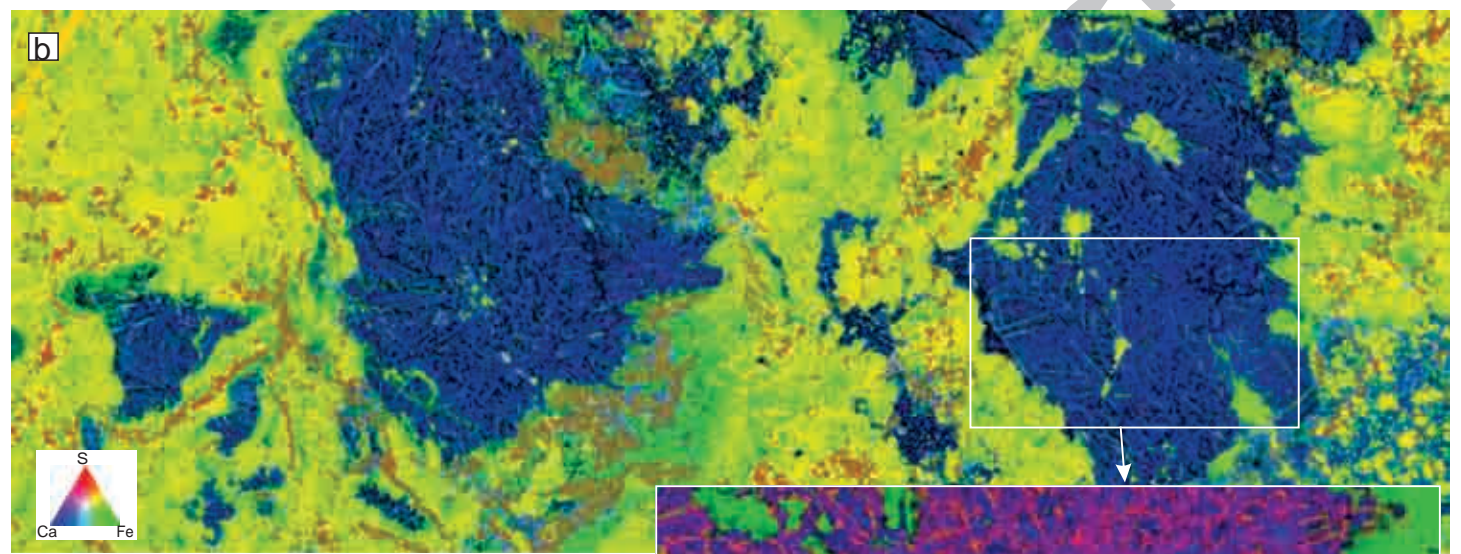


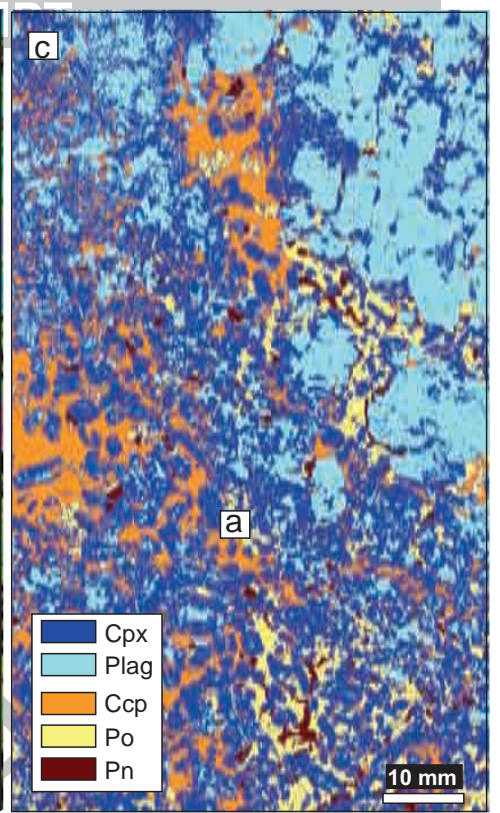
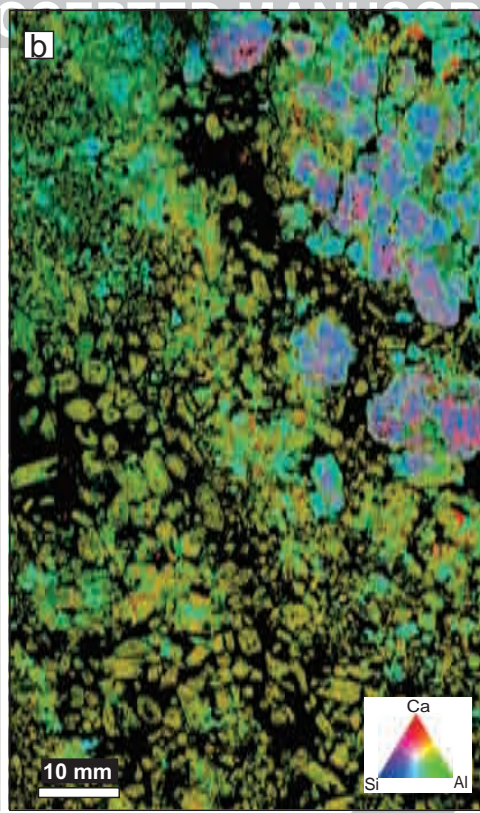




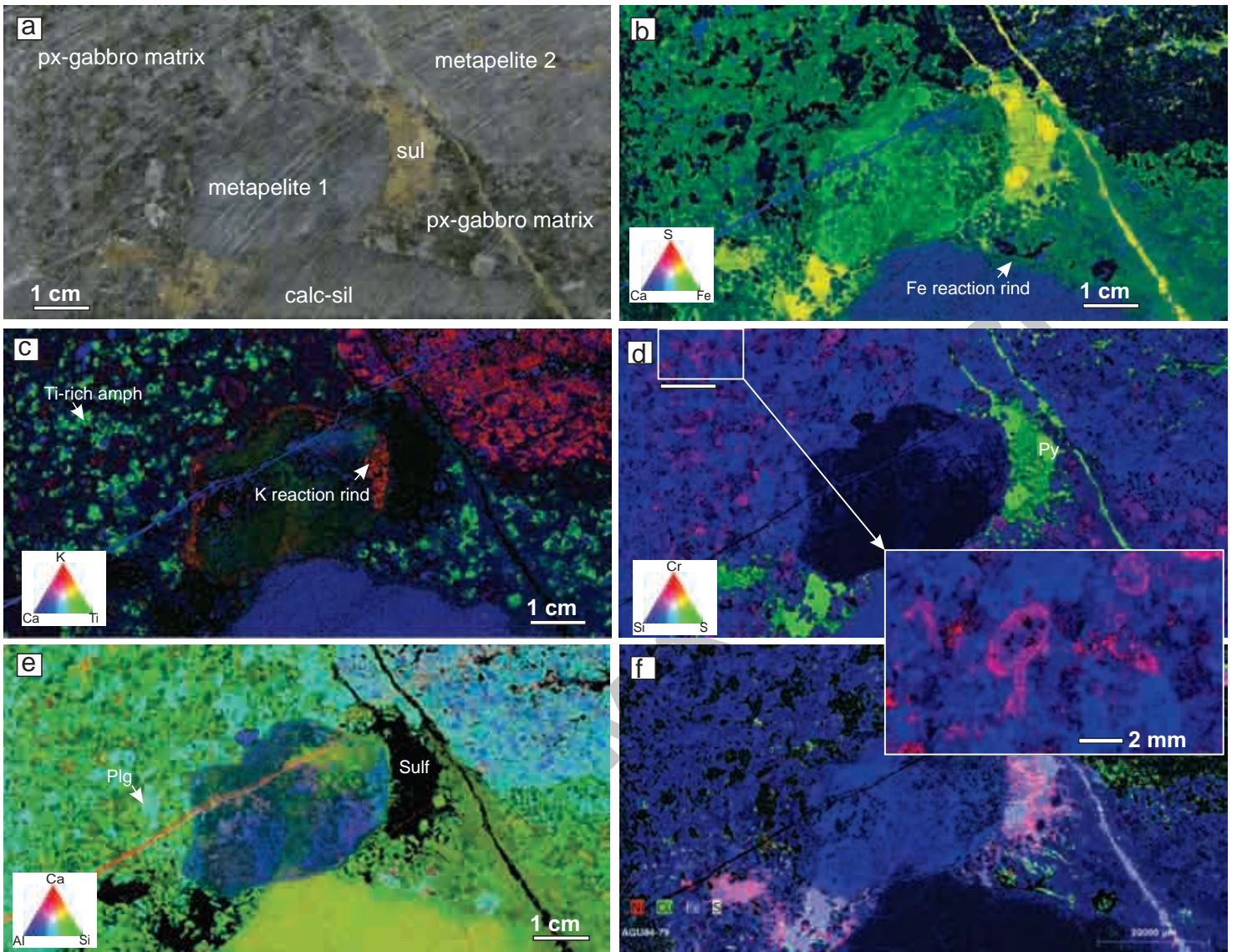




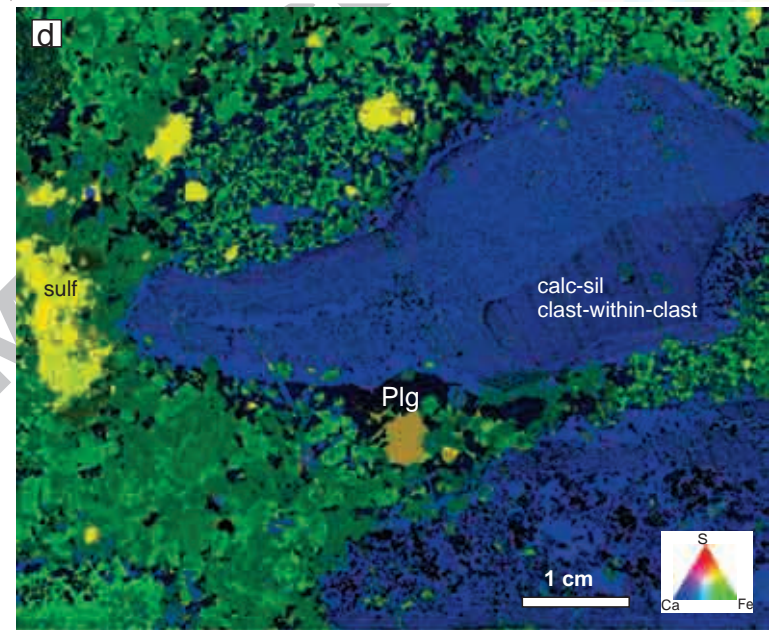
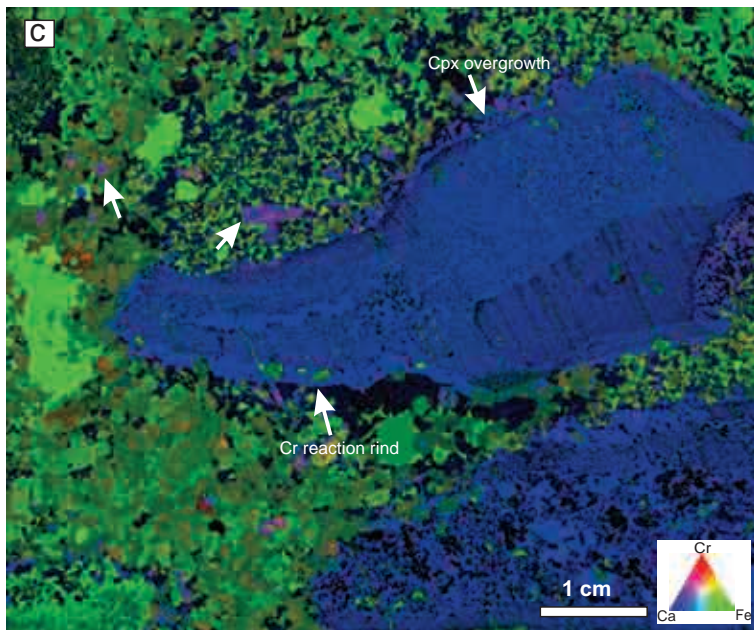
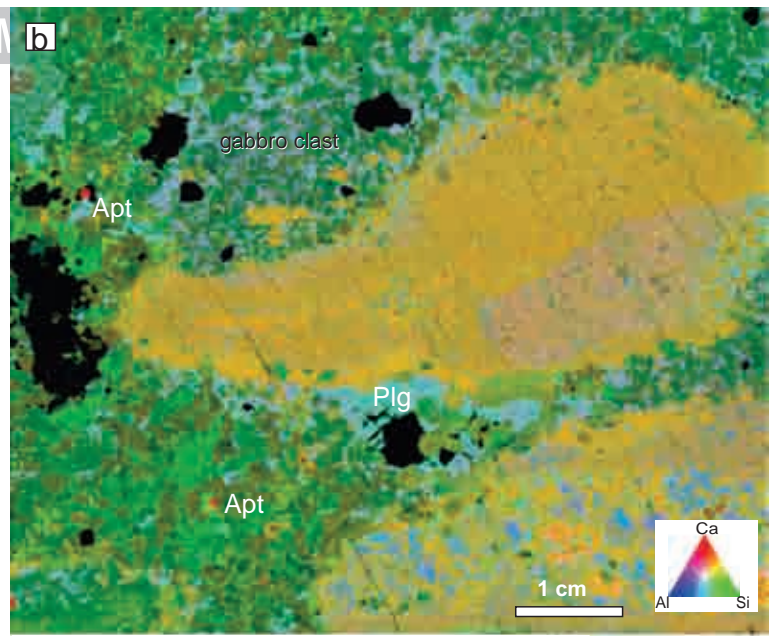




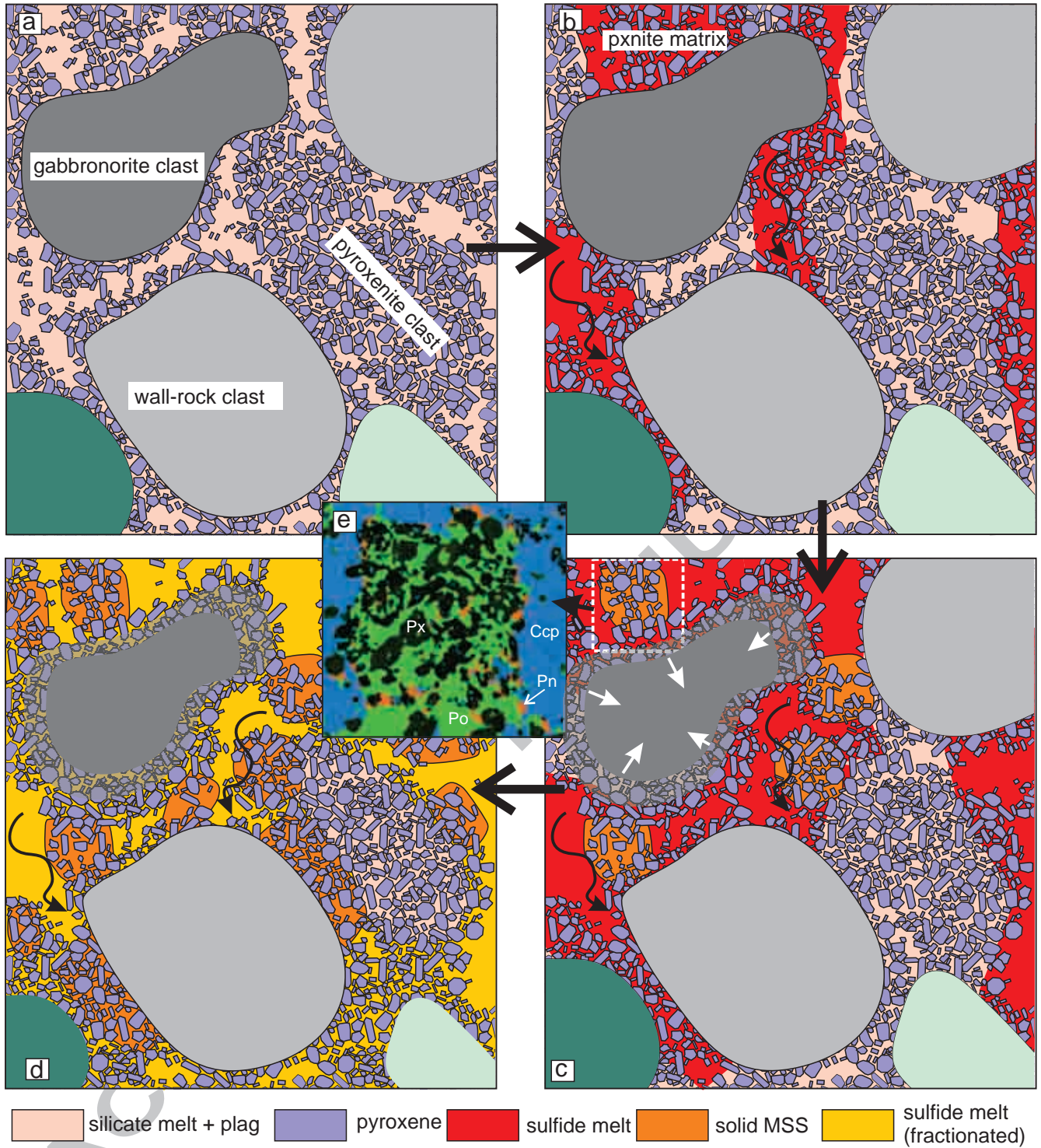
ACCEPTED MANUSCRIPT

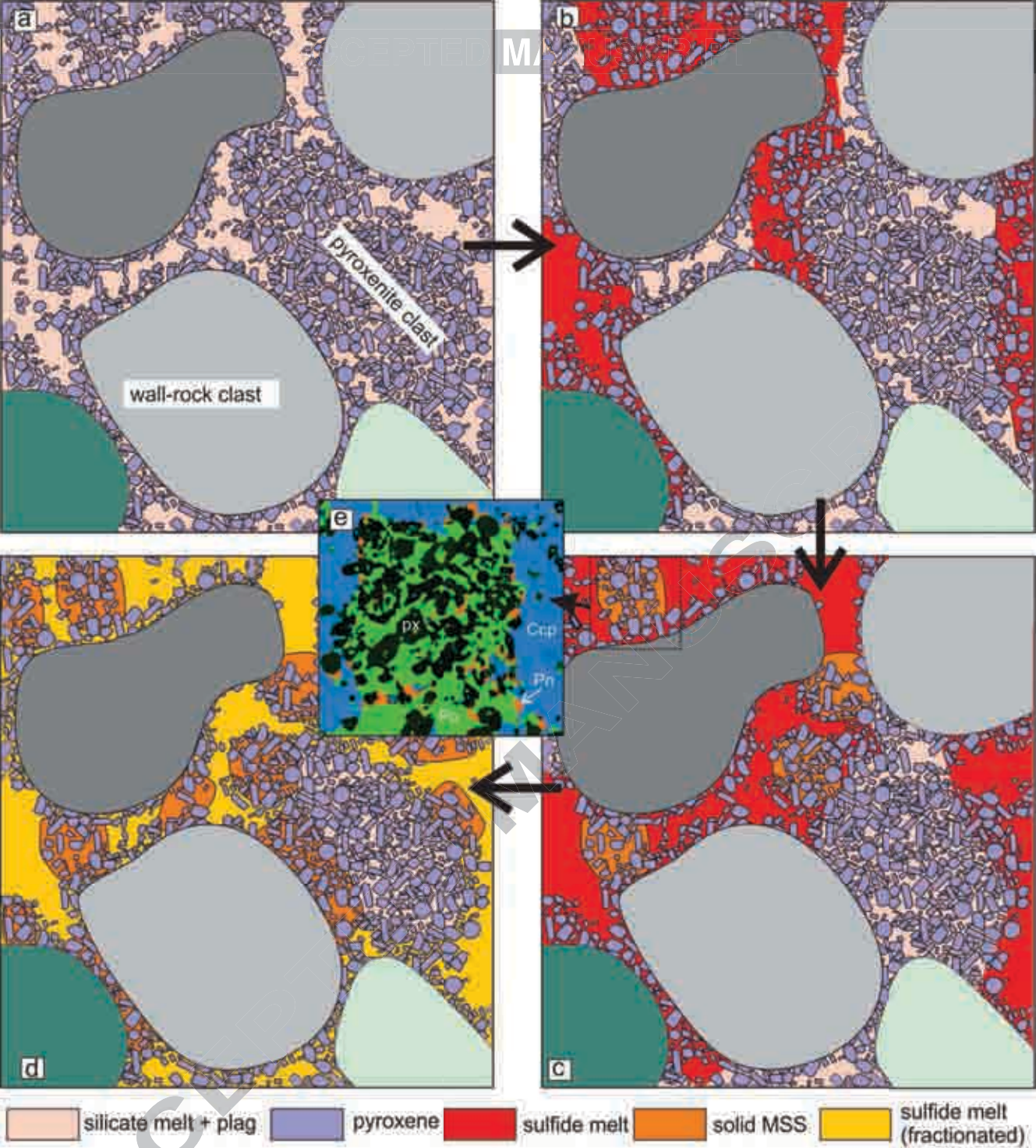


ACCEPTED



ACCEPTED





Cartoon showing model for development of sulfide-matrix breccias at Aguablanca. See text for further explanation.

- a) Breccia consisting of polymict assemblage of ultramafic, anorthositic, gabbroic and country-rock clasts in matrix of partially solidified pyroxenites.
- b) Sulfide percolation through intraclast pore space – displaces silicate melt component, partially melts pyroxene-plagioclase eutectic assemblages in matrix and clast, displaced silicate melt and some pyroxene “floats” out
- c) Initial crystallisation of sulfide liquid forms large grains of MSS that trap silicate grains and prevent them from floating up through sulfide liquid; these become preserved as frameworks of (often zoned) pyroxene crystals within pyrrhotite/pentlandite aggregates.
- d) ongoing infiltration and fractional crystallisation of sulfide melt accompanied by upward displacement of remaining silicate melt and pyroxene grains not enclosed in solid MSS. Pore space becomes flooded by Cu-rich residual sulfide melt.
- e) detail of figure 2 showing pyroxene grains (black) enclosed within po+pn (original MSS, green+orange).

Highlights:

Textural development in sulfide-matrix ore breccias in the Aguablanca Ni-Cu deposit, Spain, revealed by X-ray fluorescence microscopy

Stephen J. Barnes, Rubén Piña, Margaux Le Vaillant

- Aguablanca Ni-Cu sulfide ores contain distinctive polymict sulfide-matrix breccias, as do many mafic intrusion hosted ores
- Breccias are the result of sulfide liquid infiltration into pre-existing silicate-matrix intrusion breccias, displacing original silicate melt component
- Clasts show “soft” or “hard” margins depending on lithology – mafic clasts disaggregate into individual crystals, calc-silicate rocks have sharp smooth contacts inherited from partial dissolution.
- Breccias emplaced into neck of partially solidified funnel-shaped intrusion during late-stage backflow in a conduit system.